PCCP

Physical Chemistry Chemical Physics

www.rsc.org/pccp

Volume 15 | Number 3 | 21 January 2013 | Pages 705–1036

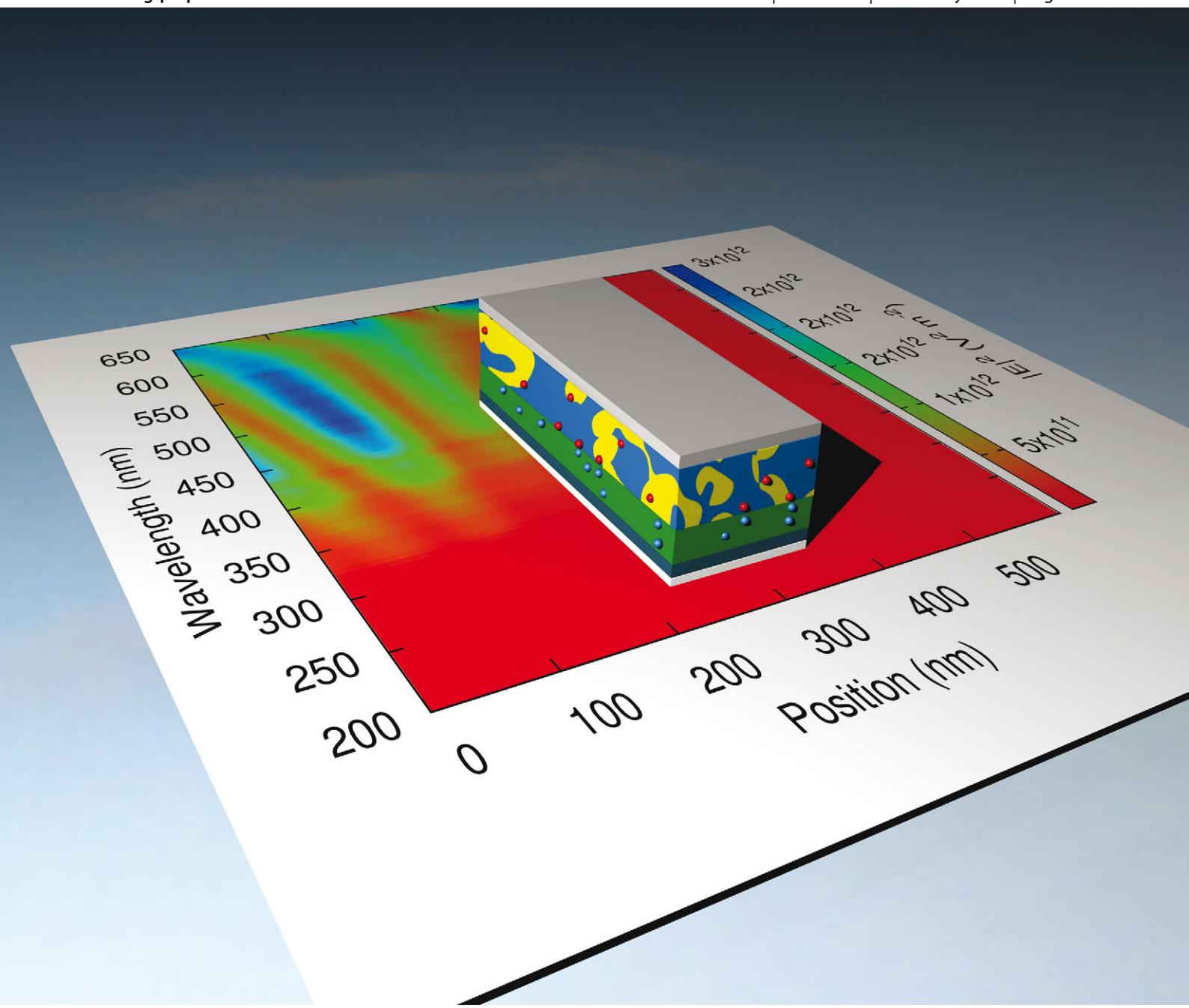

ISSN 1463-9076

PAPER

MacKenzie *et al.*

Increasing organic solar cell efficiency with polymer interlayers

1463-9076(2013)15:3;1-J

PCCP

RSC Publishing

PAPER

View Article Online
View Journal | View Issue

Increasing organic solar cell efficiency with polymer interlayers†

Cite this: *Phys. Chem. Chem. Phys.*, 2013, **15**, 764

Felix Deschler,[a] Daniel Riedel,[a] Bernhard Ecker,[b] Elizabeth von Hauff,[bc] Enrico Da Como[ad] and Roderick C. I. MacKenzie*[ef]

Received 1st November 2012,
Accepted 6th November 2012

DOI: 10.1039/c2cp43876c

www.rsc.org/pccp

We demonstrate how organic solar cell efficiency can be increased by introducing a pure polymer interlayer between the PEDOT:PSS layer and the polymer:fullerene blend. We observe an increase in device efficiency with three different material systems over a number of devices. Using both electrical characterization and numerical modeling we show that the increase in efficiency is caused by optical absorption in the pure polymer layer and hence efficient charge separation at the polymer bulkheterojunction interface.

1 Introduction

Organic solar cells have recently shown great promises as a low cost source of low carbon electricity, their efficiencies have rapidly improved from 3% in 2007[1] to over 10% today.[2] There has been much work done on optimizing all aspects of organic photovoltaic devices (OPVs) including; development of narrow bandgap polymers to improve light absorption;[3] developing better contacts[4,5] to replace expensive Indium Tin Oxide;[6,7] and development of faster production technologies to reduce the fabrication cost.[8–10] However the cost per Watt of energy produced with an organic solar cell is still not competitive to silicon[2,11] and for OPV devices to become commercially viable, improvements still need to be made in both efficiency and cost.

In the following pages we demonstrate how a significant improvement in device efficiency can be achieved by replacing a 30 nm layer of the bulk heterojunction material next to the PEDOT:PSS layer with a pure polymer layer (see Fig. 1). It is found that by introducing this layer of conjugate polymer the energy conversing efficiency can be reliably increased for cells made from three different material systems. Furthermore, as this polymer layer replaces a section of the bulkheterojunction layer containing expensive fullerene, the total fabrication cost of the new solar cell can be reduced.

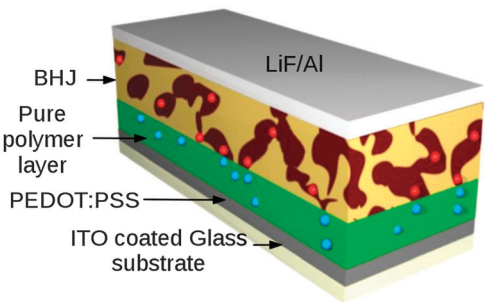

Fig. 1 A diagram of the more efficient bi-layer structure. A polymer layer is used to replace a 30 nm section of the BHJ. This reduces the amount of fullerene used and increases solar cell efficiency. The blue spheres represent holes and the red spheres represent electrons.

The paper is divided into three sections; first we describe the fabrication process of the bi-layer structures as depicted in Fig. 1, next we characterize the devices using Impedance Spectroscopy (IS), steady state electrical measurements and transient optoelectronic techniques. We then extend our electro-optical device model[12] to simulate carrier transport over heterojunctions[13–15] and optical propagation/carrier generation in multilayered structures. Finally using a combination of characterization and modeling we show that the increased efficiency is due to optical generation of excitons within the polymer layer and subsequent charge separation at the polymer:fullerene interface. Hereafter, the solar cell structure with the polymer layer will be referred to as the bi-layer structure and the normal structure will be referred to as the mono-layer structure.

2 Experimental

Three polymer:fullerene material systems were investigated; poly(3-hexylthiophene):phenyl-C61-butyric acid methyl ester (P3HT:PCBM); poly[(4,40-bis(2-ethylhexyl)dithiene[3,2-*b*:20,30-d]silole)-2,6-diyl-*alt*-(4,7-bis(2-thienyl)-2,1,3-benzothiadiazole)-5,50-diyl] (Si-PCPDTBT:

[a] *Department of Physics and CeNS, Ludwig-Maximilians-Universtität München, Amalienstr. 54, D-80799 München, Germany*
[b] *Institute of Physics, Hermann-Herder-Str. 3a, Freiburg, D-79104, Germany*
[c] *Fraunhofer Institute for Solar Energy Systems (ISE), Heidenhofstr. 2, Freiburg, D-79110, Germany*
[d] *Department of Physics, University of Bath, Somerset, BA2 7AY, UK*
[e] *FRIAS, School of Soft Matter Research, University of Freiburg, Albertstraße 19, Freiburg, 79104, Germany*
[f] *Faculty of Engineering, University of Nottingham, Nottingham, Nottinghamshire NG7 2RD, UK. E-mail: roderick.mackenzie@nottingham.ac.uk*

† Electronic supplementary information (ESI) available. See DOI: 10.1039/c2cp43876c

PCBM); and Poly[[4,8-bis[(2-ethylhexyl)oxy]benzo[1,2-*b*:4,5-*b*′]dithiophene-2,6-diyl][3-fluoro-2-[(2-ethylhexyl)carbonyl]thieno[3,4-*b*]thiophenediyl]] (PTB7:PCBM). Mono-layer devices and bi-layer devices were fabricated from each material system, in the bi-layer devices the polymer layer was made from the same polymer as was used in the bulk-heterojunction. A picture of a bi-layer device is shown in Fig. 1. The detailed fabrication of the devices is described in the ESI.† For characterization, the solar cells were mounted in a sealed box providing inert atmosphere to prevent degradation and masking of the active area, defining three solar cells, each with pixel sizes of 0.125 cm^2. The light and dark *JV*-characteristics were measured using a source-measure unit (Keithley 2400), illumination was provided through a solar simulator (LOT-Oriel) equipped with filters maintaining an AM 1.5G spectrum. The intensity was set to 100 mW cm^{-2} using a calibrated silicon reference diode. The transient photovoltage measurements were carried out using a Xenon high pressure lamp with different illumination intensities for background illumination. A diode pumped passively Q-switched laser (FTSS 355-50, CryLas GmbH) with a pulse length around 1 ns and a wavelength of 532 nm was used to perturbate the solar cell held at open circuit with the internal 1 M Ω impedance of an oscilloscope.

The resulting transients were recorded using a digital oscilloscope (DPO 7254, Tektronix). For impedance spectroscopy[16] a potentiostat system (Autolab PGSTAT302N, Metrohm) equipped with an impedance module, controlled *via* NOVA software, was used. The complex resistance was recorded from 1 MHz down to 10 Hz at an applied AC voltage of 30 mV (RMS). The solar cells were either kept in dark or illuminated by high brightness LEDs with varying illumination intensities together with an superimposed DC voltage equal to the respective V_{oc}.

3 Results

3.1 Statistical *JV* curve measurement

Fig. 2a and b plot the efficiency and fill factor (FF) of a series of devices made from P3HT:PCBM, Si-PCPDTBT:PCBM and PTB7:PCBM. It can be seen that all polymer:fullerene systems with the polymer layer deposited between the PEDOT:PSS interlayer and the BHJ (bi-layer devices) outperform devices made from a single BHJ (mono-layer devices). The fill factor is also observed to increase, this could be a sign of less recombination or a higher average shunt resistance. Fig. 2c and d plot the short circuit and open circuit voltage of the devices. It can be seen that the open circuit voltage hardly changes when the polymer layer is added, this suggests that recombination is not significantly changed by the polymer layer.[17] However, the short circuit current does increase across all devices with the bi-layer structure suggesting that carrier photo-generation is increasing with the addition of the bi-layer.

Published on 07 November 2012.

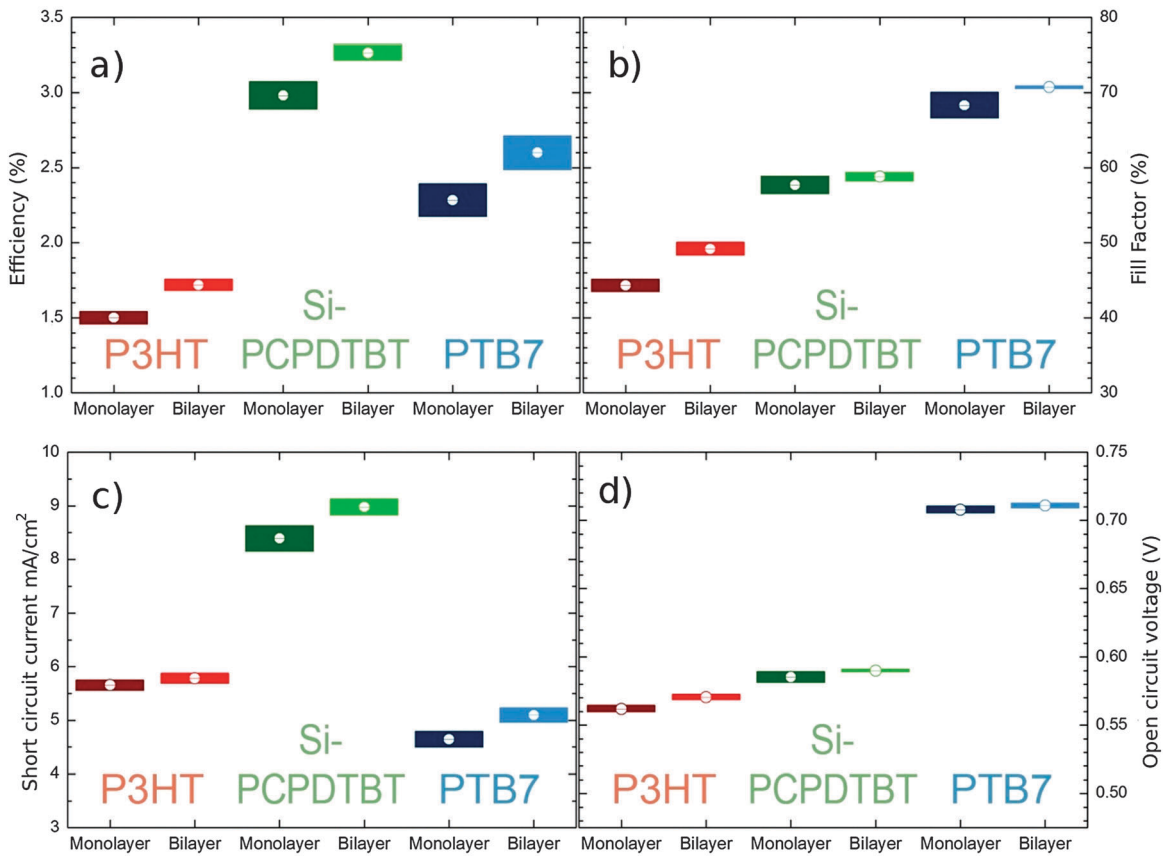

Fig. 2 Efficiency (a), fill factor (b), Open circuit voltage (c) and circuit current (d) plotted for P3HT:PCBM, Si-PCPDTBT:PCBM and PTB7:PCBM devices for mono-layer and bi-layer structures. Data points are averaged over 30 devices.

3.2 Analysis of dark *JV* curves and recombination data

One possible reason for the increase in device efficiency could be a reduction in recombination in the device, possibly caused by the polymer layer filling in any imperfections/holes in the PEDOT:PSS layer, thus preventing electrons reaching the ITO layer. To test this thearom recombination was measured in the device using Transient Photovoltage (TPV)[18] and Impedance Spectroscopy (IS).[19] The measured carrier lifetimes are plotted in Fig. 3. It can also be seen that that the transient photovoltage lifetimes for the mono-layer and bi-layer devices are very similar, suggesting that the increase in efficiency is not due to decreased recombination. It can also be seen that the TPV measurements and the IS measurements produce exactly the same carrier lifetimes thus confirming the results.

Typical dark *JV* curves for the P3HT:PCBM and PTB7:PCBM devices are plotted in Fig. 4. It can be seen that both the bi-layer devices have a higher shunt resistance than the mono-layer devices. The mono-layer devices have a shunt resistance of $3 \times 10^4\ \Omega$ and the bi-layer devices have a shunt resistances of $1 \times 10^4\ \Omega$. This suggests that the polymer layer is helping increase the shunt resistance by eliminating short circuits between the contacts, this could be a possible cause for the increased efficiency of the devices. However, it is not clear from these results alone that the increased shunt resistance is the only reason for the increased device efficiency.

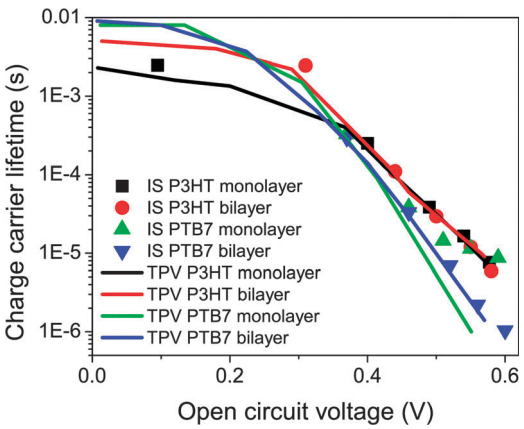

Fig. 3 Carrier lifetimes measured by TPV and IS for P3HT:PCBM and PTB7:PCBM systems.

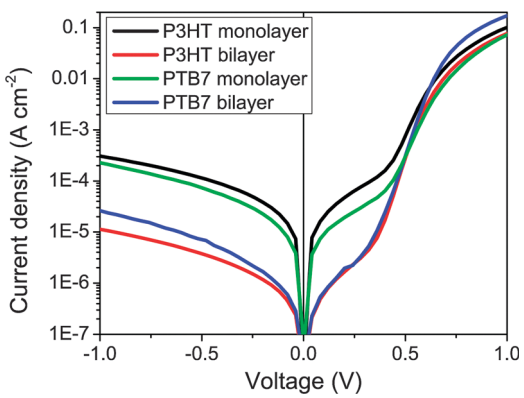

Fig. 4 Dark *JV* curves for the mono-layer and bi-layer structures made from P3HT:PCBM and PTB7:PCBM. The polymer layer increases the shunt resistance.

4 Theoretical analysis

In order to better understand the reason for the increased efficiency of the bi-layer devices, we develop a numerical device model capable of simulating both the electrical and optical properties of the bi-layer structures. We then fit this model to a representative light and dark *JV* curves from a P3HT:PCBM mono-layer cell. The result of the fit and model parameters are given in the ESI.† In the following sections, we first describe the device model we then use this calibrated model along with electrical characterization to investigate the cause of the increase in device efficiency in the bi-layer systems.

4.1 The model

To describe transport and electrostatic effects within the device Poisson's equation and the bi-polar drift-diffusion equations are solved in 1D.[12] For the mono-layer structure the electrical model was solved over the BHJ layer alone while for the bi-layer the model was solved over the polymer layer and the BHJ. Recombination[20–25] and carrier trapping[26–30] are described using the Shockley–Read–Hall[31–33] recombination mechanism which has recently been shown capable of describing both steady state and transient behavior of OPV devices.[12] Recombination in OPV devices has been shown to occur *via* carrier trap states and that an exponential distribution of states can reproduce experimental data well,[17,34–36] we therefore choose an exponential distribution LUMO (PCBM) and HOMO (polymer) trap states. Only these two orbitals are considered since they are responsible for transport, trapping and recombination of polarons. Parasitic shunt and series resistances are added to the ideal diode model. The model has been described in detail elsewhere.[12]

Fig. 5 plots a typical trapped carrier distribution as simulated by the model for a bi-layer structure in position and energy space under 1 Sun illumination at open circuit. The pure polymer layer can be clearly seen on the left hand side of the picture as an offset in band gap where the LUMO of P3HT is used instead of the LUMO of PCBM. The offset in band gap results in a reduction of electrons density close to the hole rich contact, due to the increased distance between then hole quasi-Fermi level the

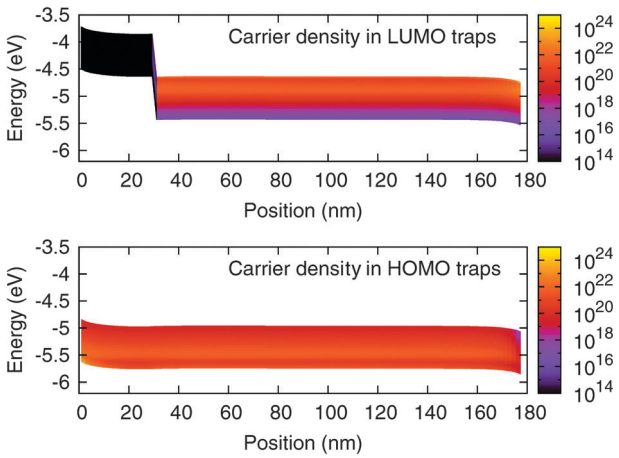

Fig. 5 Energy and position space plot of carrier density within the simulated device. The polymer layer can clearly be seen on the left hand side of the device. It can be seen that the pure polymer layer has a very a low electron density.

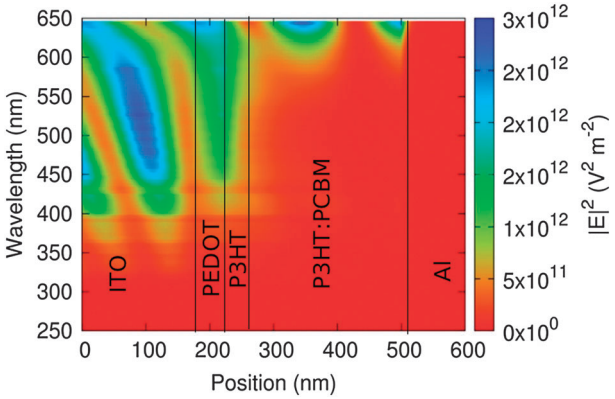

Fig. 6 The photon distribution within the devices as a function position and wavelength.

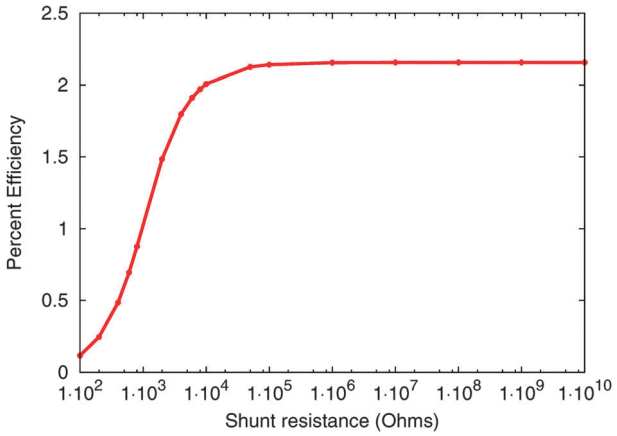

Fig. 7 Device efficiency plotted against shunt resistance. The mono-layer devices have a low shunt resistance, this was boosted with the introduction of the bi-layer.

Published on 07 November 2012.

electron band edge. This reduction in electron population can be seen as an un-populated area in the graph which is colored black. This low electron density in the pure polymer layer results in a very low carrier recombination rate is low within this layer.

The optical field profile within the device was calculated by assuming the incident radiation on the cell is transversely polarized to the interfaces. Then the forward and backward propagating fields across the all material interfaces were forced to be continuous. Phase shifts and absorption are taken into account assuming an exponential dependence of field on propagation distance in the complex plane. The optical model is solved over all material layers within the device, the differences in refractive index and absorption were taken to account using the following previously published data (ITO[37]/PEDOT:[37]PSS/P3HT[37,38]/P3HT:PCBM[38]/LiF/Al[39]). The influence of the glass substrate was neglected and a 1.5 AM optical spectrum was used as the light source. This method is identical to the transfer matrix method[40] however all equations are solved on a finite difference grid within one matrix to minimize the computational effort (see ESI†). A typical field profile calculated as a function of position and wavelength is shown in Fig. 6, it can be seen that in this example there is a high photon density in the pure P3HT polymer layer.

4.2 Analysis of increased shunt resistance caused by the polymer layer

To investigate if the change in shunt resistance could explain the increase in device efficiency, a series of *JV* curves were simulated with the calibrated model using different shunt resistances and the resulting device efficiency plotted. The results can be seen in Fig. 7. It can be seen that for shunt resistances under $1 \times 10^6\ \Omega$ the shunt resistance has an influence on device efficiency. However the difference in efficiency between a device with a shunt resistance of $3 \times 10^4\ \Omega$ and $1 \times 10^6\ \Omega$ is only 0.1%. This is not enough to explain the observed 0.25% increase in efficiency shown in Fig. 2. Furthermore, we were unable to explain the increase in short circuit current with an increase in shunt resistance alone.

4.3 Optical effects caused by the polymer-layer

In the previous sections we demonstrated that the increase in device efficiency can not be explained by electrical effects within the device alone. This leaves optical effects left to be investigated.

When PCBM is mixed with P3HT to form a blend the resulting film is optically less dense over the solar spectrum than a film of pure P3HT because the absorption of PCBM is weak below 400 nm and does not coincide with the maxima in the solar spectra.[38] Thus one would expect the pure polymer layer of P3HT in the bi-layer structure to absorb a significant amount of solar radiation. This is confirmed by the optical simulation plotted in Fig. 8. It can be seen that very little light is absorbed in the ITO/PEDOT:PSS layers, however a significant amount of light is absorbed in the 30 nm thick P3HT layer. Indeed the peak photon absorption in the polymer layer is higher than in the peak photon absorption in the BHJ of the mono-layer or bi-layer device. Table 1 plots the percentage of light absorbed in each layer of the bi-layer device shown in Fig. 8. It can be seen that the P3HT layer absorbs 21.70% of the total light and accounts for 40% of the light absorbed in the electrically active layer. From Fig. 8, it can also be seen that the addition of the polymer-layer significantly reduces the light absorbed within the BHJ. Thus the light absorbed in the polymer-layer must contribute to the photocurrent or the cell efficiency would decrease with the addition of the polymer layer. This in turn

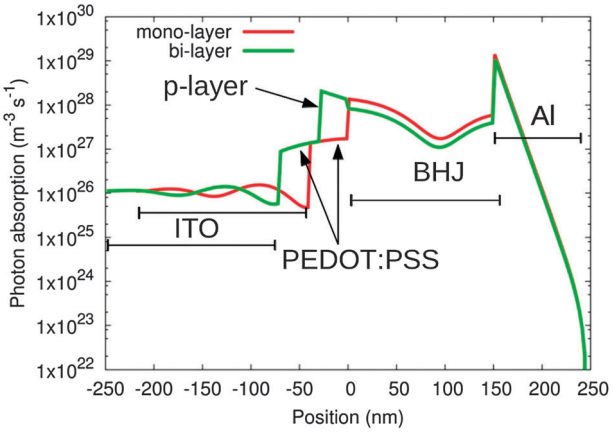

Fig. 8 The photon absorption within the device as a function of position summed over the spectrum. It can be seen that a significant amount of light is absorbed in the pure polymer layer, therefore, for the bi-layer devices to have an increased efficiency the excitons generated within this layer must be split and reach the contacts as current.

Table 1 Absorption within the layers. The pure polymer layer absorbs a significant amount of light −40% of the light absorbed within the active layers

Layer	Percent of light absorbed
ITO	0.9%
PEDOT:PSS	2.19%
P3HT	21.70%
P3HT:PCBM	31.38%
Al	43.84%

suggests that excitions generated in the polymer layer diffuse to the polymer/polymer:fullerene interface where disassociation takes place.

4.4 Electrical and optical effects caused by the polymer-layer

In this section we use the model to understand how exciton generation in the polymer layer and the subsequent splitting of the excitions at the polymer/BHJ interface, will affect the device efficiency. The exciton diffusion length in P3HT has been reported to range between 5 nm[41] and 27 ± 12 nm.[42] Therefore in the model we take the diffusion length to be 30 nm and assume that photon which is absorbed within 30 nm of the P3HT:PCBM interface will be able to diffuse to the interface and generate an electron hole pair, with an electron being generated in the PCBM LUMO and a hole in the pure P3HT layer HOMO. Any photon which is absorbed more than 30 nm away from the interface will be recombine and not generate photocurrent.

Initially full electrical and optical simulations were performed to predict the efficiency in mono-layer devices with different BHJ thicknesses. The results from these simulations are shown in Fig. 9 as the continuous red line between 10 nm and 300 nm. It shows that when the BHJ is very thin the device efficiency is very low, because the device can not absorb much light. As the BHJ thickness is increased the device absorbs more light and thus the efficiency also increases. However, as the device gets thicker it is more probable that a photogenerated carrier will recombine before leaving the device, thus after 170 nm the device no longer becomes more efficient with increasing BHJ thicknes. Further simulations were performed for bi-layer devices where the thickness of the BHJ was held constant (at 40 nm, 80 nm, 120 nm, 160 nm, 200 nm and 240 nm) while varying the width of the polymer-layer. These simulations are plotted on top of the red curve in Fig. 9. It can be seen that bi-layer devices outperform devices consisting of only a BHJ of the same thickness. This is because the step in the LUMO at the polymer/BHJ interface prevents electrons entering the polymer-layer thus reduces the recombination rate within the polymer-layer. The polymer-layer thus allows for higher rates of charge generation without high rates of recombination which would be associated with the higher charge density/photo current in a normal BHJ. Fig. 10 plots the recombination within a bi-layer device as a function of position at open circuit.

It can also be seen from Fig. 9 that once the polymer-layer thickness is larger than the exciton diffusion length the device efficiency starts to decrease. This is because the polymer layer absorbs photons but the generated excitons geminately recombine before reaching the polymer/BHJ interface. Thus, to achieve an optimum device the polymer-layer thickness must be tuned to the excition diffusion length.

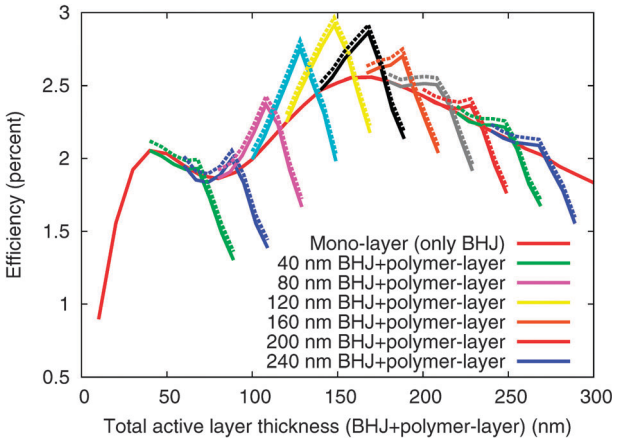

Fig. 9 A plot of device efficiency against total active layer thickness (BHJ + polymer layer). The red line stretching from 10 nm to 300 nm shows a device with no polymer layer consisting of a BHJ only. The other lines represent devices formed from BHJs of different set thicknesses (40 nm, 80 nm, 120 nm, 160 nm, 200 nm and 240 nm) with varying thickness polymer-layers added to the structures. It can be seen that the addition of pure polymer layer with a thickness matching the exciton diffusion length can significantly increase device efficiency. The dotted lines show the impact of increasing the shunt resistance from 3×10^4 Ω to 1×10^6 Ω.

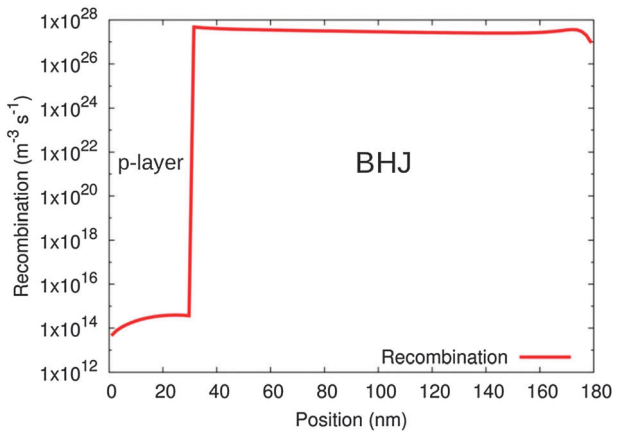

Fig. 10 Recombination as a function of position within the device at V_{oc}. There is very little recombination within the p-layer due to the heterojunction at the polymer/BHJ interface.

5 Conclusion

In this work we demonstrate that by adding a pure polymer-layer between the PEDOT:PSS and the BHJ layers in organic solar cells made from P3HT:PCBM, Si-PCPDTBT:PCBM and PTB7:PCBM, device performance can be improved. We demonstrate the bi-layer increases shunt resistance in the device but apart from that no other electrical changes are observed. We further demonstrate that a significant proportion of light is absorbed within the polymer layer and this must turn into photocurrent for an increase in cell efficiency. The bi-layer structure offers two key advantages over the normal BHJ structure; (a) It increases device efficiency; and (b) less fullerene is needed for the active layer which is expected to reduce overall cost of the device. This strategy for increasing the energy conversion efficiency is expected to work in other polymer:PCBM systems and

Published on 07 November 2012.

further increases in efficiency are expected to be gained by using a wide bandgap polymer such as P3HT for the p-layer and a narrow bandgap polymer for the bulk-heterojunction.

Acknowledgements

R. MacKenzie gratefully acknowledges the support of FRIAS. We wish to thank Imperial College High Performance Computing Service for providing computational support. D. Riedel and F. Deschler fabricated the devices and performed the statistical *JV* curve measurements, B. Ecker performed the IS analysis, and R. MacKenzie performed the numerical modeling, TPV measurements and wrote the manuscript. We thank Lukas Smidt-Mende for access to the solar cell characterization equipment. More applications of the model described within this paper can be found at www.opvdm.com.

References

1 M. A. Green, K. Emery, Y. Hishikawa and W. Warta, *Prog. Photovoltaics*, 2007, **15**, 425–430.
2 M. A. Green, K. Emery, Y. Hishikawa and W. Warta, *Prog. Photovoltaics*, 2011, **19**, 84–92.
3 C. H. Woo, P. M. Beaujuge, T. W. Holcombe, O. P. Lee and J. M. J. Frechet, *J. Am. Chem. Soc.*, 2010, **132**(44), 15547–15549.
4 M. W. Rowell, M. A. Topinka, M. D. McGehee, H.-J. Prall, G. Dennler, N. S. Sariciftci, L. Hu and G. Gruner, *Appl. Phys. Lett.*, 2006, **88**(23), 233506.
5 B. Zimmermann, H.-F. Schleiermacher, M. Niggemann and U. Wrfel, *Sol. Energy Mater. Sol. Cells*, 2011, **95**(7), 1587–1589.
6 K. P. Musselman, T. Gershon, L. Schmidt-Mende and J. L. MacManus-Driscoll, *Electrochim. Acta*, 2011, **56**(11), 3758–3763.
7 H. C. Hesse, D. Lembke, L. Dssel, X. Feng, K. Mllen and L. Schmidt-Mende, *Nanotechnology*, 2011, **22**(5), 055303.
8 M. M. Voigt, R. C. Mackenzie, C. P. Yau, P. Atienzar, J. Dane, P. E. Keivanidis, D. D. Bradley and J. Nelson, *Sol. Energy Mater. Sol. Cells*, 2011, **95**(2), 731–734.
9 M. M. Voigt, R. C. Mackenzie, S. P. King, C. P. Yau, P. Atienzar, J. Dane, P. E. Keivanidis, I. Zadrazil, D. D. Bradley and J. Nelson, *Sol. Energy Mater. Sol. Cells*, 2012, **105**, 77–85.
10 F. C. Krebs, S. A. Gevorgyan, B. Gholamkhass, S. Holdcroft, C. Schlenker, M. E. Thompson, B. C. Thompson, D. Olson, D. S. Ginley, S. E. Shaheen, H. N. Alshareef, J. W. Murphy, W. J. Youngblood, N. C. Heston, J. R. Reynolds, S. Jia, D. Laird, S. M. Tuladhar, J. G. Dane, P. Atienzar, J. Nelson, J. M. Kroon, M. M. Wienk, R. A. Janssen, K. Tvingstedt, F. Zhang, M. Andersson, O. Ingans, M. Lira-Cantu, R. de Bettignies, S. Guillerez, T. Aernouts, D. Cheyns, L. Lutsen, B. Zimmermann, U. Wrfel, M. Niggemann, H.-F. Schleiermacher, P. Liska, M. Grtzel, P. Lianos, E. A. Katz, W. Lohwasser and B. Jannon, *Sol. Energy Mater. Sol. Cells*, 2009, **93**(11), 1968–1977.
11 C. J. Emmott, A. Urbina and J. Nelson, *Sol. Energy Mater. Sol. Cells*, 2012, **97**, 14–21.
12 R. C. I. MacKenzie, C. G. Shuttle, M. L. Chabinyc and J. Nelson, *Adv. Energy Mater.*, 2012, **2**(6), 662–669.
13 R. MacKenzie, J. J. Lim, S. Bull, S. Sujecki, A. J. Kent and E. C. Larkins, *J. Phys.: Conf. Ser.*, 2007, **92**(1), 012068.
14 J. Lim, R. MacKenzie, S. Sujecki, M. Sadeghi, S. Wang, G. Adolfsson, Y. Wei, A. Larsson, P. Melanen, P. Uusimaa, A. George, P. Smowton and E. Larkins, *Opt. Quantum Electron.*, 2008, **40**, 385–390.
15 R. MacKenzie, J. Lim, S. Bull, S. Chao, S. Sujecki, M. Sadeghi, S. Wang, A. Larsson, P. Melanen, P. Sipila, P. Uusimaa and E. Larkins, *IET Optoelectron.*, 2007, **1**(6), 284–288.
16 T. Kirchartz, W. Gong, S. A. Hawks, T. Agostinelli, R. C. I. MacKenzie, Y. Yang and J. Nelson, *J. Phys. Chem. C*, 2012, **116**(14), 7672–7680.
17 T. Kirchartz, B. E. Pieters, J. Kirkpatrick, U. Rau and J. Nelson, *Phys. Rev. B: Condens. Matter Mater. Phys.*, 2011, **83**(11), 115209.
18 C. G. Shuttle, R. Hamilton, B. C. O'Regan, J. Nelson and J. R. Durrant, *Proc. Natl. Acad. Sci.*, 2010, **107**(38), 16448–16452.
19 P. P. Boix, J. Ajuria, R. Pacios and G. Garcia-Belmonte, *J. Appl. Phys.*, 2011, **109**(7), 074514.
20 M. Hilczer and M. Tachiya, *J. Phys. Chem. C*, 2010, **114**(14), 6808–6813.
21 C. Groves and N. C. Greenham, *Phys. Rev. B: Condens. Matter Mater. Phys.*, 2008, **78**(15), 155205.
22 M. Hilczer and M. Tachiya, *J. Phys. Chem. C*, 2010, **114**(14), 6808–6813.
23 L. J. A. Koster, V. D. Mihailetchi and P. W. M. Blom, *Appl. Phys. Lett.*, 2006, **88**(5), 052104.
24 R. A. Street, *Phys. Rev. B: Condens. Matter Mater. Phys.*, 2011, **84**(7), 075208.
25 A. Wagenpfahl, C. Deibel and V. Dyakonov, *IEEE J. Sel. Top. Quantum Electron.*, 2010, **16**(6), 1759–1763.
26 H. Bassler, *Phys. Status Solidi B*, 1993, **175**, 15–55.
27 B. Bohnenbuck, E. von Hauff, J. Parisi, C. Deibel and V. Dyakonov, *J. Appl. Phys.*, 2006, **99**(2), 024506.
28 Y. Roichman and N. Tessler, *Appl. Phys. Lett.*, 2002, **80**(11), 1948–1950.
29 F. F. Stelzl and U. Würfel, *Phys. Rev. B: Condens. Matter Mater. Phys.*, 2012, **86**, 075315.
30 N. Tessler and Y. Roichman, *Org. Electron.*, 2005, **6**(56), 200–210.
31 W. Shockley and W. T. Read, *Phys. Rev.*, 1952, **87**(5), 835–842.
32 L. Tzabari and N. Tessler, *J. Appl. Phys.*, 2011, **109**(6), 064501.
33 W. Tress, K. Leo and M. Riede, *Phys. Rev. B: Condens. Matter Mater. Phys.*, 2012, **85**, 155201.
34 R. C. I. MacKenzie, T. Kirchartz, G. F. A. Dibb and J. Nelson, *J. Phys. Chem. C*, 2011, **115**(19), 9806–9813.
35 J. Nelson, *Phys. Rev. B: Condens. Matter Mater. Phys.*, 2003, **67**(15), 155209.
36 A. Foertig, J. Rauh, V. Dyakonov and C. Deibel, *Phys. Rev. B: Condens. Matter Mater. Phys.*, 2012, **86**, 115302.
37 G. Dennler, K. Forberich, M. C. Scharber, C. J. Brabec, I. Tomis, K. Hingerl and T. Fromherz, *J. Appl. Phys.*, 2007, **102**(5), 054516.
38 V. Shrotriya, J. Ouyang, R. J. Tseng, G. Li and Y. Yang, *Chem. Phys. Lett.*, 2005, **411**(1–3), 138–143.
39 A. D. Rakić, *Appl. Opt.*, 1995, **34**(22), 4755–4767.
40 G. F. Burkhard, E. T. Hoke and M. D. McGehee, *Adv. Mater.*, 2010, **22**(30), 3293–3297.
41 O. V. Mikhnenko, H. Azimi, M. Scharber, M. Morana, P. W. M. Blom and M. A. Loi, *Energy Environ. Sci.*, 2012, **5**, 6960–6965.
42 S. Cook, H. Liyuan, A. Furube and R. Katoh, *J. Phys. Chem. C*, 2010, **114**(24), 10962–10968.